Computers & Fluids 71 (2013) 272–282

Contents lists available at SciVerse ScienceDirect

Computers & Fluids

journal homepage: www.elsevier.com/locate/compfluid

Evaluation and improvements of RANS turbulence models for linear diffuser flows

Christian Heschl [a,*], Kiao Inthavong [b], Wolfgang Sanz [c], Jiyuan Tu [b]

[a] Fachhochschule Burgenland, University of Applied Science, Steinamangerstraße 21, Pinkafeld 7423, Austria
[b] School of Aerospace, Mechanical and Manufacturing Engineering, RMIT University, PO Box 71, Plenty Road, Bundoora, Victoria 3083, Australia
[c] Institute for Thermal Turbomachinery and Machine Dynamics, Graz University of Technology, Inffeldgasse 25, Graz 8010, Austria

ARTICLE INFO

Article history:
Received 13 July 2012
Received in revised form 10 October 2012
Accepted 18 October 2012
Available online 8 November 2012

Keywords:
CFD
Mixed ventilation
Indoor airflow
Anisotropic
RANS

ABSTRACT

Flow patterns produced by linear diffusers are highly dependent on the turbulent momentum exchange process. Hence a realistic computation of indoor room airflows that are produced from plane wall and free jets requires an accurate prediction of the anisotropic turbulent stresses. This is particularly the case in regions near the wall and entrainment effects which are caused by the turbulent shear stresses. For this reason a non-linear eddy viscosity assumption is presented which can be adjusted to account for the turbulent mixing process in the free shear flow region, and to reproduce the redistribution of the turbulent normal stresses near the wall. Based on several test cases such as a free and plane wall jet, IEA (International Energy Agency) Annex 20 room airflow, and a 3D room with a partition, the essential characteristics of the linear and non-linear k–ε, k–ω and v^2–f turbulence models are analysed. Thereby it is shown that the proposed non-linear assumption can improve the prediction of linear diffuser airflows.

1. Introduction

Ventilation systems that use linear diffusers, supply air at relatively high velocity at or around the ceiling producing a rich variety of flow features such as turbulent jets, flow recirculation, flow separation and reattachment. Recent research in building and indoor airflows have shown that Computational Fluid Dynamics (CFD) simulations can play an important role in ventilation design for buildings, evident by the number of building related CFD papers tripling over the period between 1985 and 2003 [38].

Due to the lower computational effort most airflow simulations are based on the Reynolds Averaged Navier Stokes (RANS) equations with a first-order-closure turbulence model using a linear correlation between the Reynolds stress tensor and the strain rate tensor (i.e. the Boussinesq approach). This leads to the so-called RANS turbulence models which exhibit inherent isotropic behaviour thus producing erroneous flow predictions in the near wall region and for high shear, strain and swirling flows. In linear diffuser flows where an air inlet is mounted next to a surface, a wall jet arises and the redistribution of the turbulent normal stresses produces a large lateral redistribution of the flow which is not captured by linear turbulence models [2,22]. Therefore continuing research is needed in order to understand the behaviour and performance of available turbulence models for such airflows.

In review papers by Chen and Zhai [6], and Zhang et al. [39], it was concluded that the accuracy and reliability of CFD simulations significantly depend on the chosen turbulence model in order to account for the turbulent and transitional flow regimes that exist in indoor airflows. Chung [8] used the standard linear k–ε model to simulate the flow in a partitioned enclosed room and showed that the computed results of temperature and velocity fields agreed well with measured data. Other studies found that the RNG-k–ε variant displayed satisfactory agreement with experimental data [1,7]. Chen [5] evaluated five k–ε models including the standard and RNG model for predicting natural and forced convection flows, and found that for the RNG model: (i) the prediction of mean velocity is more accurate than that of the turbulent velocity, (ii) anisotropic turbulence leading to secondary recirculation of indoor airflow was not captured, and (iii) the RNG k–ε model is slightly better than the standard k–ε model and is therefore recommended for indoor airflow simulations. The fact that the RNG k–ε model performs better than the standard k–ε model is also confirmed by Rouaud and Havet [29] and Gebremedhin and Wu [14], based on simulations on different geometries.

The k–ω turbulence models are less popular for indoor room flows despite its capabilities in handling boundary layer flows. The only study found in literature using the k–ω model was by Gebremedhin and Wu [14] which found the standard k–ω model to be unsuitable for a model office room, whereas the k–ω-SST model showed the best agreement with measurements compared to laminar, standard k–ε and RNG k–ε models. Given the lack of data with the k–ω-SST model, a systematic approach to evaluate the model for standard test cases that feature flow characteristics

* Corresponding author. Tel.: +43 3357 45370 1321.
E-mail addresses: christian.heschl@fh-pinkafeld.ac.at (C. Heschl), kiao.inthavong@rmit.edu.au (K. Inthavong), wolfgang.sanz@tugraz.at (W. Sanz), jiyuan.tu@rmit.edu.au (J. Tu).

0045-7930/$ - see front matter © 2012 Elsevier Ltd. All rights reserved.
http://dx.doi.org/10.1016/j.compfluid.2012.10.015

found in mixed ventilation system is needed. Peng et al. [27] investigated the performance of the standard k–ε, k–ω, and a modified k–ω model and found that their modified version of the k–ω model gave similar predictive accuracy to the k–ε model but faster convergence.

In order to contribute more knowledge towards better indoor airflow modeling, this paper systematically investigates the performance of existing RANS turbulence models for linear diffuser flows. Improvements to the standard linear RANS models by using their non-linear enhancements are proposed and implemented to evaluate their performance in predicting airflow fields typically produced by these diffusers. Development of the non-linear model is described, where the model constants are calibrated based on measurement and DNS data. Evaluation of the models are performed on standard and well-defined geometries which includes: (i) 2D free and plane wall jets to determine the ability of exchange of turbulence in the free shear flow field (i.e. entrainment), (ii) a 2D confined ventilated room (IEA-Annex 20 room), and (iii) a 3D room with a partition.

2. Turbulence models

2.1. Linear eddy viscosity models

The steady-state continuity and momentum equations based on the RANS equations for incompressible fluids and isothermal flow are

$$\frac{\partial u_j}{\partial x_j} = 0 \tag{1}$$

$$\bar{u}_j \frac{\partial u_i}{\partial x_j} = -\frac{1}{\rho}\frac{\partial p}{\partial x_i} + \frac{\partial}{\partial x_j}\left[\nu \frac{\partial u_i}{\partial x_j}\right] - \frac{\partial \overline{u_i' u_j'}}{\partial x_j} \tag{2}$$

In most RANS turbulence models the Reynolds stresses $-\rho\overline{u_i' u_j'}$ are modelled in analogy to a Newtonian isotropic fluid by multiplying the strain rate tensor S_{ij} by a linear turbulent viscosity which is a product of a turbulent length scale L_t, a turbulent velocity scale U_t, density ρ and a model constant C_μ.

$$-\rho\overline{u_i' u_j'} = \rho C_\mu L_t U_t S_{ij} - \frac{2}{3}\rho k \delta_{ij} \tag{3}$$

where k is the turbulent kinetic energy defined as $k = 0.5\ \overline{u_k' u_k'}$. The turbulent length scale can be substituted by the turbulent time scale T_t and the turbulent viscosity μ_t can be expressed as

$$\mu_t = \rho C_\mu L_t U_t = \rho C_\mu U_t^2 T_t \tag{4}$$

To close the linear eddy viscosity model the turbulent velocity scale and the turbulent length or time scale must be known. This can be found by additional transport equations for the necessary turbulent quantities. The turbulence models and their respective equations that will be used in this study are given in Table 1.

2.2. Non-linear RANS models

The turbulent stresses in Eq. (3) are linearly related to the velocity gradients found in the strain rate tensor S_{ij}. Non-linear RANS models include non-linear terms of the strain-rate for the definition of the Reynolds stresses. Thus the Reynolds stresses can be based on the Reynolds stress anisotropy tensor b_{ij} as

$$b_{ij} = \frac{\overline{u_i' u_j'}}{2k} - \frac{1}{3}\delta_{ij} \tag{5}$$

In principle nonlinear eddy viscosity models assume that the anisotropy tensor depends on the local velocity gradients and the turbulent time scale. In the literature a large number of such algebraic Reynolds stress models are available [4], while other models are based on the constitutive equations from Shih et al. [31]. In principle the non-linear models can be summarized in the following form

$$b_{ij} = \sum_\lambda G_\lambda T_{ij}^\lambda \qquad T_{ij} = T_{ij}(S_{ij}, \Omega_{ij}, T_t) \tag{6}$$

where G_λ are model constants, T_{ij} is a nonlinear function of the local velocity gradients expressed by the shear rate tensor S_{ij} and the vorticity tensor Ω_{ij}, T_t is the turbulent time scale; for a non-linear k–ε model $T_t = k/\varepsilon$, and for a nonlinear k–ω model $T_t = 1/\omega$. Therefore the anisotropic tensor is only determined by the local velocity gradients (S_{ij} and Ω_{ij} respectively) and the turbulent time scale. The required model constants G_λ must be specifically adapted for the considered flow situation. In this context it should be noted that the numerical stability of non-linear models is strongly influenced by the chosen values G_λ, thus the choice of the model constants G_λ should be made carefully.

In this paper, airflows with free shear flow and wall affected areas are considered. For this reason a second order nonlinear approach is sufficient to reproduce the turbulent shear and the anisotropic normal stresses. For the modeling of the Reynolds stress anisotropy tensor b_{ij} the approach of Gatski and Speziale [13] is used, where

$$b_{ij} = G_1 T_t S_{ij} + G_2 T_t^2\left(S_{ik}S_{kj} - \frac{1}{3}S_{kl}S_{kl}\delta_{ij}\right) + G_3 T_t^2(\Omega_{ik}S_{kj} - \Omega_{jk}S_{ki}) \tag{7}$$

with

$$G_1 = -C_\mu, \quad G_2 = -C_1, \quad G_3 = -C_2$$

For calibration of the model constants C_1 and C_2 existing experimental and DNS data from simple shear flows, are used. The dimensionless invariants η and ξ are used to characterise the flow parameters and are defined as

$$\eta = T\sqrt{2\ S_{ij}S_{ij}}; \qquad \xi = T\sqrt{2\Omega_{ij}\Omega_{ij}} \tag{8}$$

where

Table 1
Turbulence models and their implementation into ANSYS Fluent.

Model	Description	Abbreviation	Implementation
k–ε	Standard k–ε [20]	SKE	Default model
	Reliable k–ε [31]	RKE	Default model
	RNG [17]	RNG	Default model
k–ω	k–ε SST [23]	KW-SST	Default model
	k–ε Peng [27]	KW-Peng	User-defined-function
v^2–f	v^2–f modified by Davidson et al. [9]	V2F-Dav	User-defined-function
NL	k–ε	SKE-NL	User-defined-function
	k–ω	KW-Peng-NL	User-defined-function

Table 2
Anisotropic turbulent normal stresses for different shear flows.

Author	η rel. to ξ	b_{11}	b_{22}
Kim et al. [18]	3.30	0.179	−0.127
Tavoularis and Karnik [33]	4.30	0.220	−0.160
Tavoularis and Corrsin [32]	6.08	0.202	−0.145
de Souza et al. [10]	7.70	0.180	−0.110
Laufer [19]	3.10	0.220	−0.150

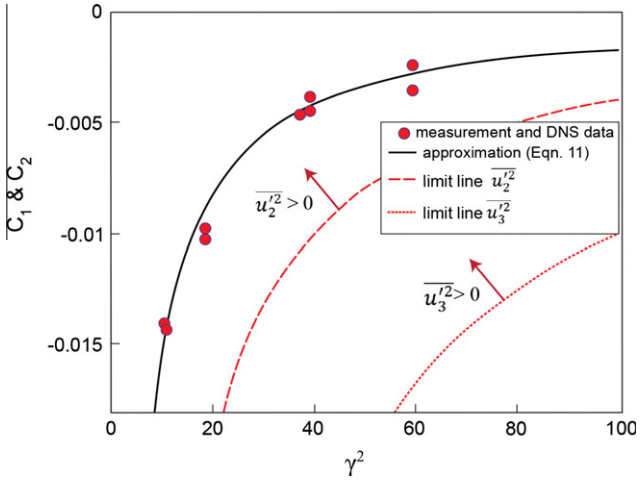

Fig. 1. Determination of the model constants C_1 and C_2.

$$S_{ij} = \left(\frac{\partial u_i}{\partial x_j} + \frac{\partial u_j}{\partial x_i}\right); \qquad \Omega_{ij} = \left(\frac{\partial u_i}{\partial x_j} - \frac{\partial u_j}{\partial x_i}\right) \tag{9}$$

Table 2 summarizes experimental and numerical data which indicate that the different anisotropic turbulent normal stresses are reproduced by different values of η and ξ. For homogeneous shear and boundary layer flows the anisotropy coefficient b_{12} is proportional to η and ξ, and the anisotropy coefficient b_{ii} to η^2 and ξ^2. It is noted that in Table 2 only the values for b_{11} and b_{22} are shown since for simple shear flows the terms $(S_{ik}S_{kj} - \frac{1}{3}S_{kl}S_{kl}\delta_{ij})$ and $(\Omega_{ik}S_{kj} - \Omega_{jk}S_{ki})$ in Eq. (7) are close to zero for $i = 1$ and $j = 2$. Therefore b_{12} becomes dependent only on C_μ, (i.e. the influence of C_1 and C_2 becomes negligible). A dimensionless invariant γ is introduced to determine the model constants C_1 and C_2, and is defined as

$$C_i = C_i(\gamma^2); \qquad \gamma = \sqrt{0.5\ (\eta^2 + \xi^2)} \tag{10}$$

The dependence of the model constants C_1 and C_2 on the dimensionless invariant γ is shown in Fig. 1 where the data points are values found from DNS and experimental data given in Table 2. The solid black line represents the corresponding approximation equation given as

$$C_1 = C_2 = \frac{-0.171}{0.9 + \gamma^2} \tag{11}$$

The results in Fig. 1 show the limits for simple shear stresses (homogeneous shear flows, two dimensional channel flow, boundary layer flows etc.), where the turbulent normal stresses $\overline{u_2'} > 0$ and $\overline{u_3'} > 0$ are positive. The comparison between the approximation in Eq. (11) and the limit lines shows that the proposed nonlinear model always predicts positive turbulent normal stresses, thus a robust and stable numerical solution is expected.

The non-linear eddy viscosity model is applied to the k–ε and k–ω turbulence model, and for boundary layer flows the quadratic terms in Eq. (7) can be neglected and a complete recalibration of the model constants $C_{1\varepsilon}$ and $C_{2\varepsilon}$ in the ε and α_∞ and β_i in the ω transport equation is not necessary. But if fine tuning is required (e.g. to improve the entrainment prediction for free jets) an individual adjustment of the model constants can be carried out by using the logarithmic wall law

$$\kappa^2 = (C_{2s} - C_{1s})\sigma_s\sqrt{C_\mu}; \qquad \alpha_\infty = \frac{\beta}{\beta_\infty^*} - \frac{\kappa^2}{\sigma_\omega\sqrt{\beta_\infty^*}} \tag{12}$$

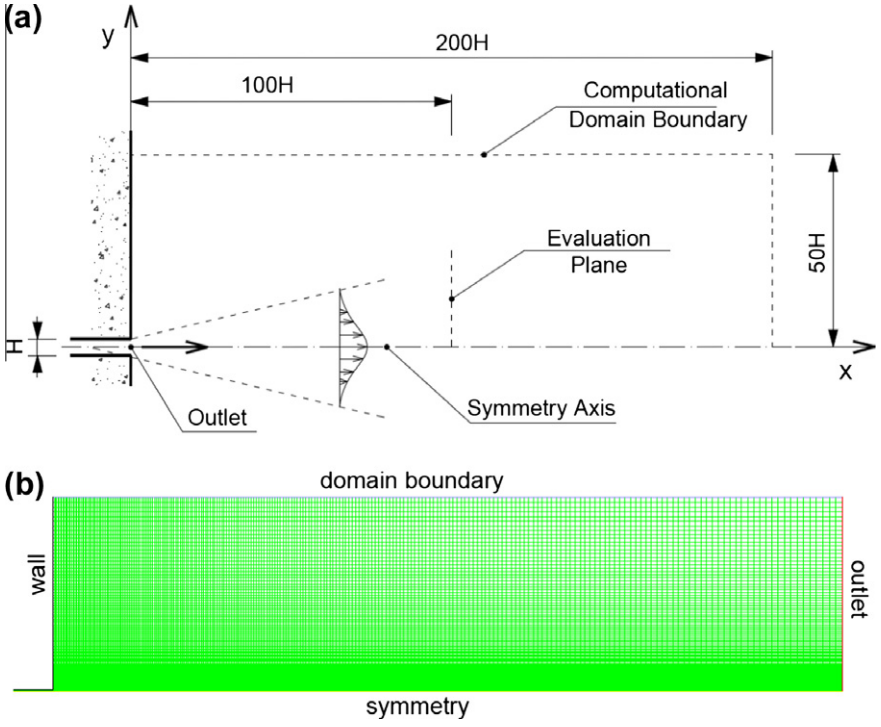

Fig. 2. (a) Computational domain of linear free jet flow including coordinates and (b) corresponding mesh modeling half the geometry.

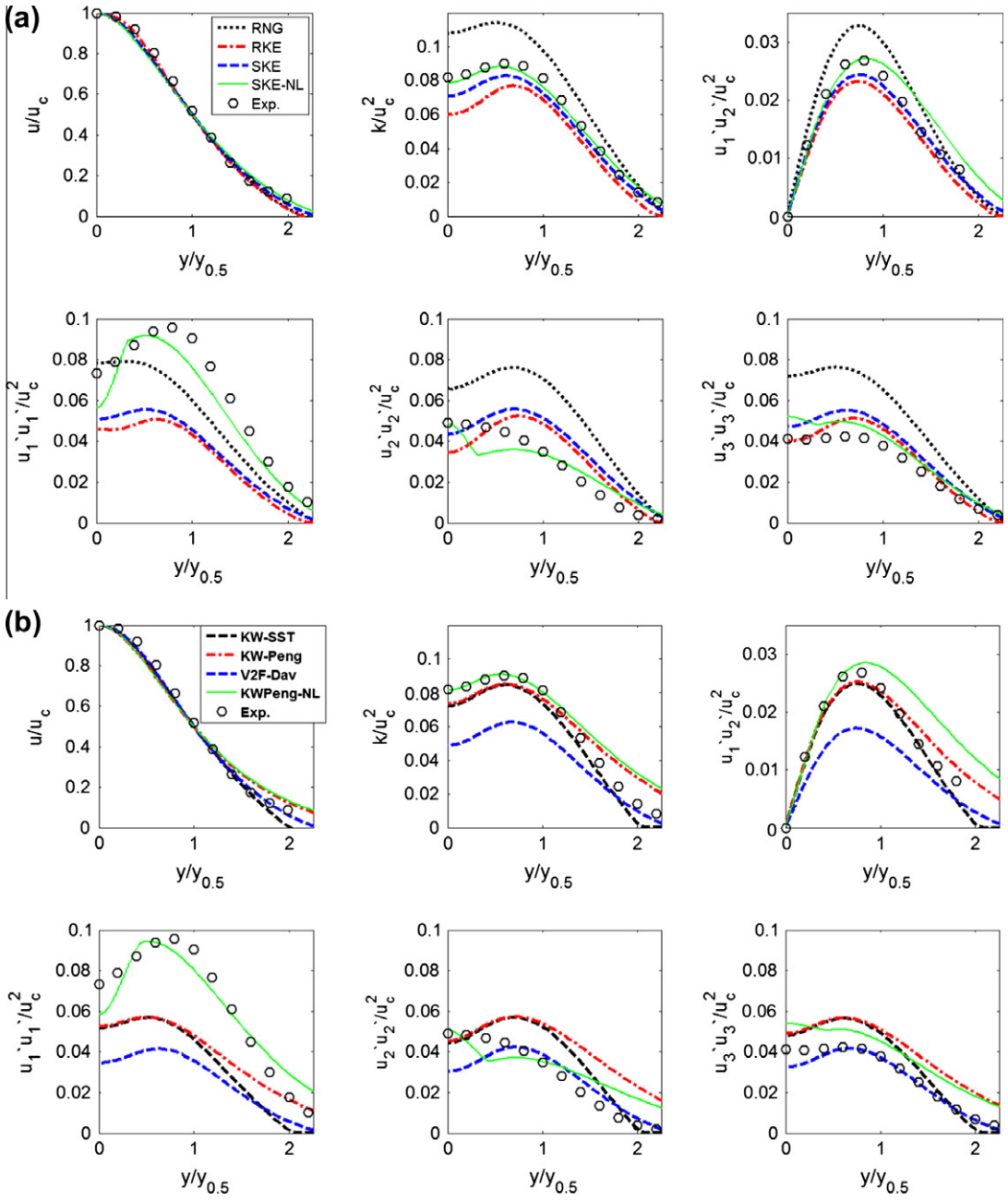

Fig. 3. Comparison of (a) k–ε turbulence models and (b) k–ω and v^2–f models with experimental data of Gutmark and Wygnanski [15].

Table 3
Comparison of calculated and measured jet spreading rate for a linear free jet.

	Exp.[a]	SKE	RNG	RKE	SKE-NL
Spreading rate	0.100	0.1101	0.1462	0.1002	0.1052
		KW-SST	KW-Peng	V2F-Dav	KW-Peng-NL
Spreading rate		0.1126	0.1153	0.0778	0.110

[a] Experimental data is taken from Gutmark and Wygnanski [15].

2.3. Implementation of the turbulence models

The turbulence models described are applied to well-defined standard geometries as they can represent critical flow features prevalent in mixed ventilation flows. These geometries include a free jet, wall jet, an indoor room flow, and 3d room with a partition which are simulated with the commercial CFD software ANSYS-Fluent. A number of built-in turbulence models are available within the software and additional models can be implemented through Fluent's direct definition for additional scalar transport

equations (i.e. the advection and diffusivity terms). Boundary conditions for the transport quantities can also be defined directly via user defined functions (UDFs).

Because the nonlinear turbulence models tend to be numerically unstable, the calculation of the production term was modified so that at the beginning of the iterations a linear correlation between the Reynolds stresses and the strain rate tensor was used. For this reason the production term was stored in a user defined memory to allow easy switching between the Boussinesq assumption and the non-linear approach of Eq. (7).

The implementation of the nonlinear eddy viscosity model into the commercial CFD code Fluent was performed using the UDF interface. The linear terms are taken into account by using the default two-equation model (SKE model). The additional quadratic terms in the non-linear models were implemented as source terms in the three momentum equations. In addition, the production terms in the transport equations of turbulent kinetic energy, dissipation rate and specific dissipation rate were adjusted by means of source terms.

The computational mesh for all models used was suitable for a low-Re calculation where the dimensionless distance to the wall of the first grid cell is $y^+ < 1$. Therefore for the k–ε models the low-Re extension proposed by Wolfshtein [37] was used. For all test cases a grid independence test based on the Richardson extrapolation [12] was carried out. In all cases a discretization error of less than 0.5% could be detected for turbulence and velocity quantities.

3. Results and discussion

3.1. Linear free jet

In the case of a turbulent free jet, ambient air is dragged into the jet which increases its mass flow, and consequently the turbulent momentum exchange during the entrainment process. Changes of flow variables along the main jet axis and the movement of the immediately surrounding air are mainly caused by the turbulent exchange processes. Therefore, a correct prediction of the projected jet spreading rate is especially important for mixing ventilation systems. The experimental investigations of Gutmark and Wygnanski [15] for a two-dimensional free jet are used as the benchmark data for validating the turbulence models. The computational domain and the mesh are shown in Fig. 2. The computational domain extends over a length of 200H and a width of 100H (based on the height H of the air inlet). To reduce the computational effort symmetry plane along the jet axis was used. The Reynolds number was 30,000 based on the height H of the air inlet and a fully developed channel flow inlet is achieved at the jet inlet by an inlet length of 50H.

The computed dimensionless profiles are shown in Fig. 3. The velocity half-width $y_{0.5}$ is thereby defined as the lateral distance from the centerline at which the local mean velocity is half the centerline value. Generally comparison between the calculated and measured dimensionless velocity profiles for all the turbulence models shows good agreement. In particular the k–ε turbulence models have a slightly better agreement in the region far from the symmetry line. The turbulent kinetic energy and shear stresses are overpredicted by the RNG model whereas the RKE, SKE, and V2F-Dav and to a lesser extent the KW-SST and KW-Peng models, underpredict these values.

Comparisons of the turbulence parameters show significant differences between the models. The profiles for the turbulent kinetic energy k and turbulent shear stress $u_1'u_2'$ are captured well by all models except by the RNG k–ε and the V2F-Dav model. The RNG turbulence model produces an overprediction of the magnitude of both k and $u_1'u_2'$ whereas the V2F-Dav model has a much lower peak value for $u_1'u_2'$. This is primarily caused by the equation determining the model constant C_{1s} which is given by

$$C_{1s} = 1.4\left(1 + 0.05\sqrt{k/v^2}\right) \tag{13}$$

This equation has been proposed in the literature in order to improve channel flow simulations [21,11], however, this leads to an underestimation of the shear stresses of free shear flows. The distribution of the turbulent normal stresses is generally poorly

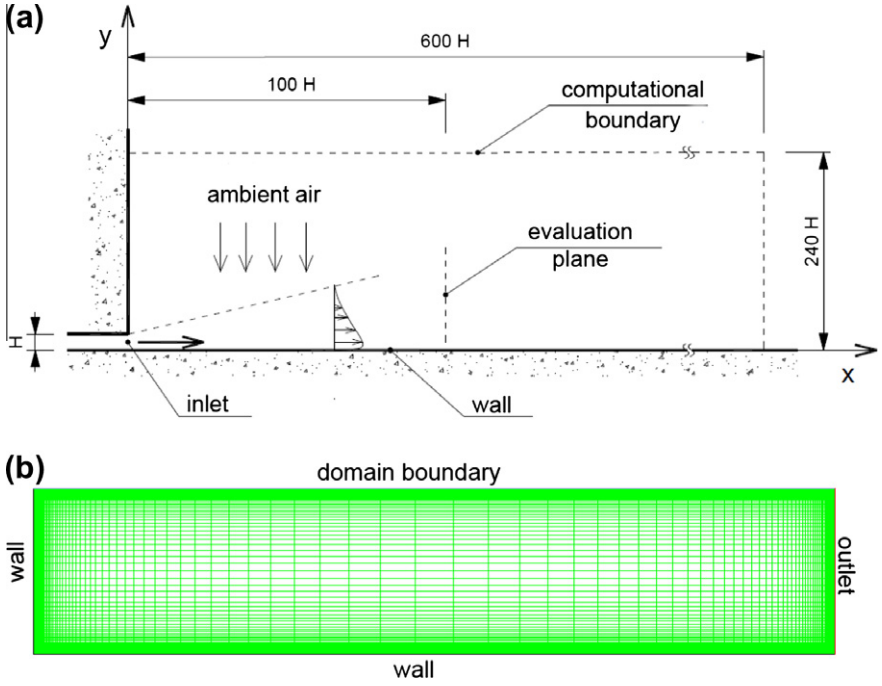

Fig. 4. (a) Computational domain of two-dimensional wall jet flow including coordinates and (b) corresponding mesh modeling half the geometry.

Table 4
Comparisons of calculated and measured jet spreading rate for a two dimensional wall jet.

	Exp[a].	SKE	RNG	RKE	SKE-NL
Spreading rate	0.081	0.0957	0.1099	0.0858	0.0919
		KW-SST	KW-Peng	V2F-Dav	KW-Peng-NL
Spreading rate		0.0741	0.0988	0.0820	0.093

[a] Experimental data from Abrahamsson [2].

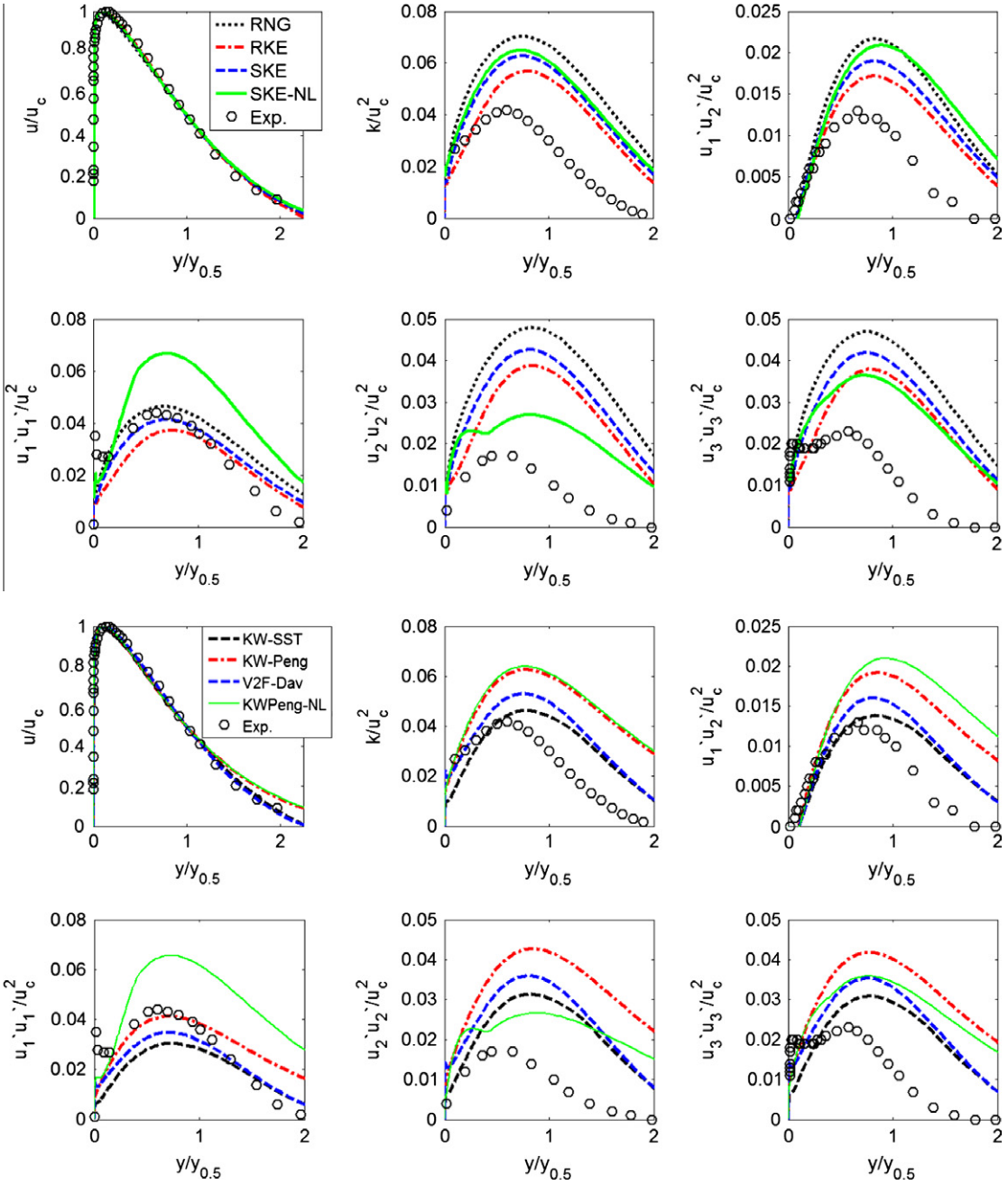

Fig. 5. Comparison of the turbulent quantities from simulations with the experimental data of Abrahamsson [2].

captured except by the non-linear models. This is most significant for the normal stress $u_1' u_2'$ where both the SKE-NL and KW-Peng-NL models show very good agreement with the experimental data.

In addition to the turbulent stresses, a key indicator of the turbulent momentum transport and the entrainment process is the jet spreading rate. It describes the change of the velocity half-width $y_{1/2}$ in the axial flow direction and is thus a measure of how much air is entrained from the environment. The jet spreading rate for the different turbulence models and their values are summarized in Table 3. Because of the direct link between the jet spreading rate

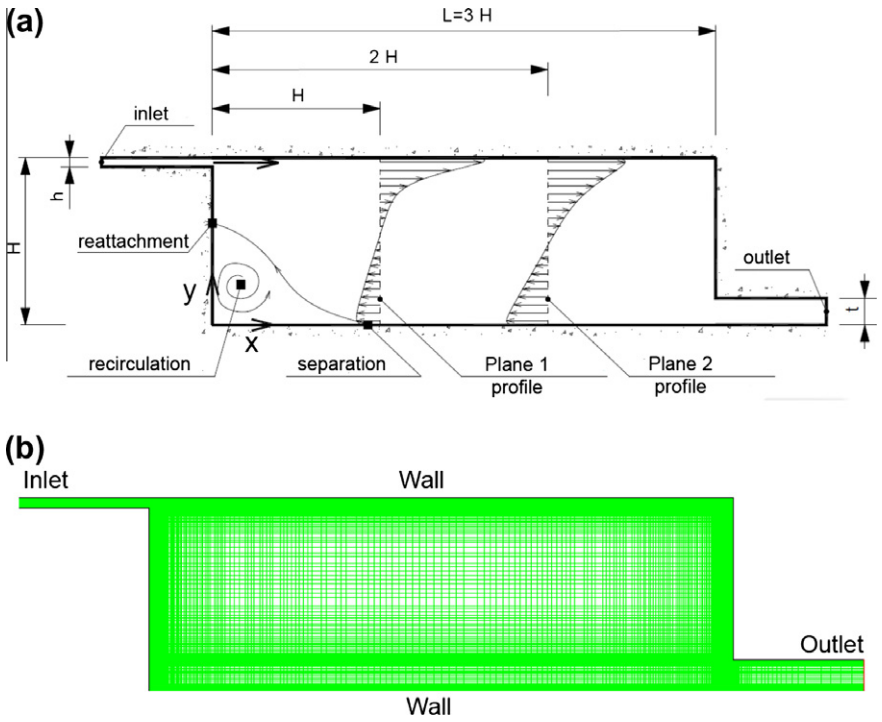

Fig. 6. (a) Geometry and arrangement of the supply and exhaust openings of the IEA Annex-20 2D room and (b) corresponding CFD mesh.

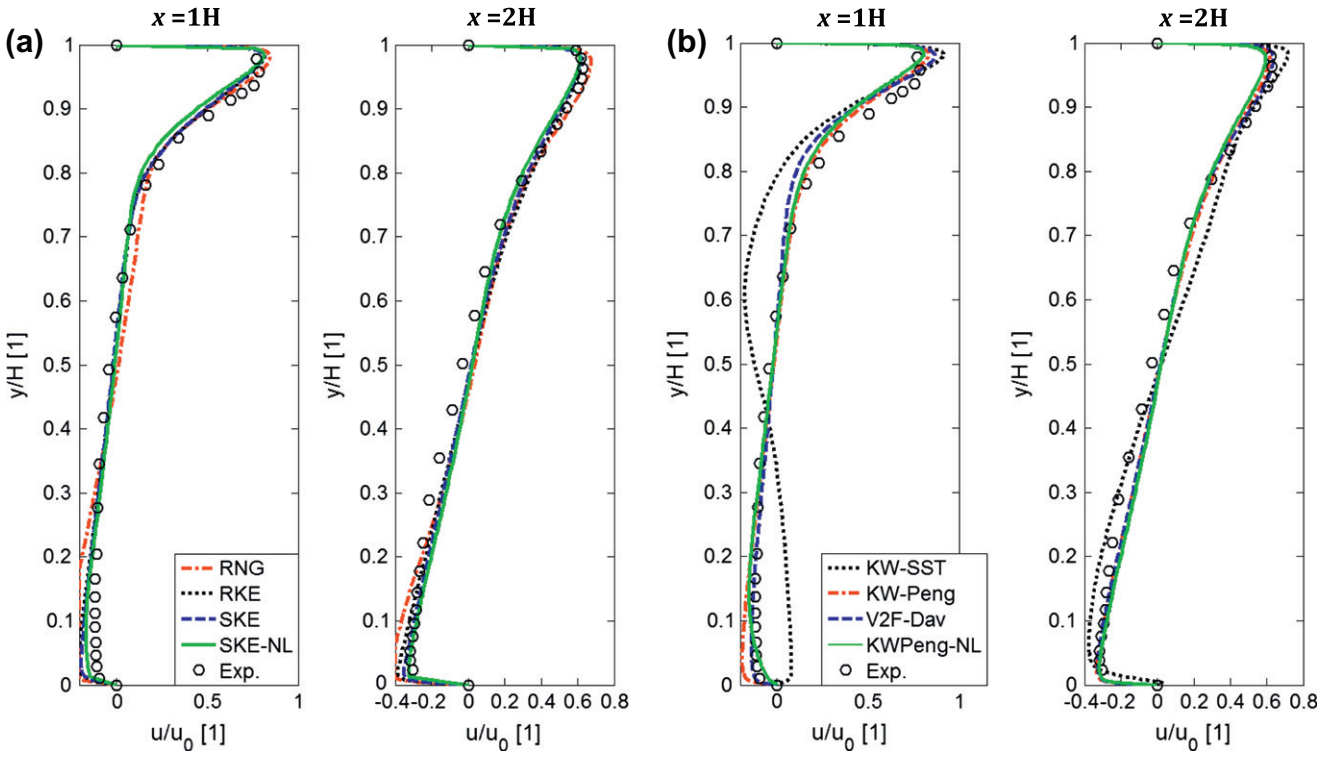

Fig. 7. Comparison of the calculated velocity profiles in 2D Annex 20 room (measurement results by Nielsen et al. [25].

and the turbulent shear stress it is expected that the results match those of its turbulence quantities. Good agreement with experimental data is achieved by the SKE, RKE, and the non-linear turbulence models. The RNG model overestimates the spreading rate, which correlates to its overprediction of $u_1'u_2'$. Conversely the V2F-Dav model underestimates the spreading rate, in correlation to its underprediction of $u_1'u_2'$.

At this point it must also be noted that the spreading rate for flat, circular and radial free jets differ from each other. Individual calibration of the proportionality factors for the model constants

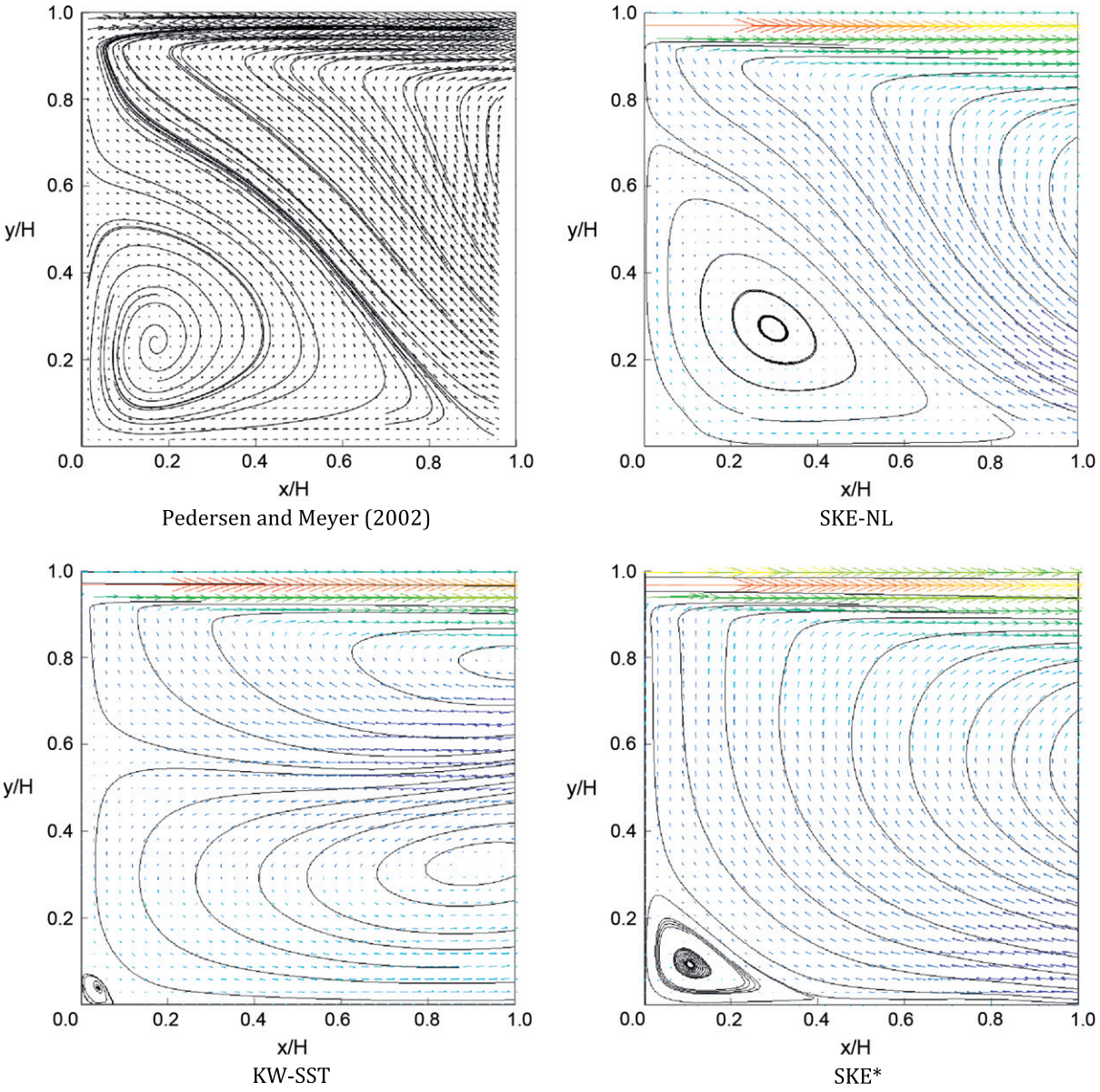

Fig. 8. Plots of velocity vectors coloured by axial velocity and overlayed with streamlines for different turbulence models and the experimental data by Pedersen and Meyer [26]. *The results for SKE model are similar to the results of RNG, RKE and V2F-DAV models.

in the production term (C_{1s} for the k–ε and α for the k–ω model) and dissipation term (C_{2s} for the k–ε and β for the k–ω model) is necessary. An alternative to individual calibration of the model constants is to include cross-diffusion terms [16] which provide some enhancements, although a general improvement is not guaranteed (the round jet/plane jet anomaly leads to the round jet/radial jet anomaly [30,36]).

3.2. Plane wall jet

In a two-dimensional wall jet, air is supplied via a slot immediately adjacent to a wall. The flow consists of an inner and an outer layer arising from the presence of the no-slip condition at the wall. The inner layer corresponds to a wall flow with a boundary layer and covers the region between the wall and the center of the jet. The adjacent outer layer corresponds to a free turbulent shear flow similar to the two-dimensional free jet. Due to the unilateral boundary wall and the associated damping of turbulence, the jet spreading rate is significantly lower than that of free jets (e.g. 2D wall jets, $dy_{1/2}/dx \approx 0.08$–0.07 compared with 2D free jets $dy_{1/2}/dx \approx 0.10$–0.11). The strong interaction between the turbulence production in the free shear layer with the turbulence damping in the wall boundary layer, is the same phenomenon that is found in flow of diffusers of mixed ventilation systems placed at ceilings. Such a flow case is therefore suitable for evaluation of the capability of different turbulence models in predicting wall-dominated air currents.

Fig. 4 shows the computational domain which consists of the inlet opening, the rear wall, the base wall, and the inlet jet that propagates along the wall. The simulations were performed for a Reynolds number of 10,000 (based on the inlet height $H = 0.01$ and the mean inlet velocity), to match with the experimental setup of Abrahamsson [3]. Jet flow profiles for the mean velocity, the turbulent kinetic energy and the turbulent stresses were taken at a distance of $x = 100H$. In addition, the calculated jet spreading rates $dy_{1/2}/dx$ is given in Table 4.

Comparison between the calculated and measured dimensionless velocity profiles shows that the linear k–ε turbulence models

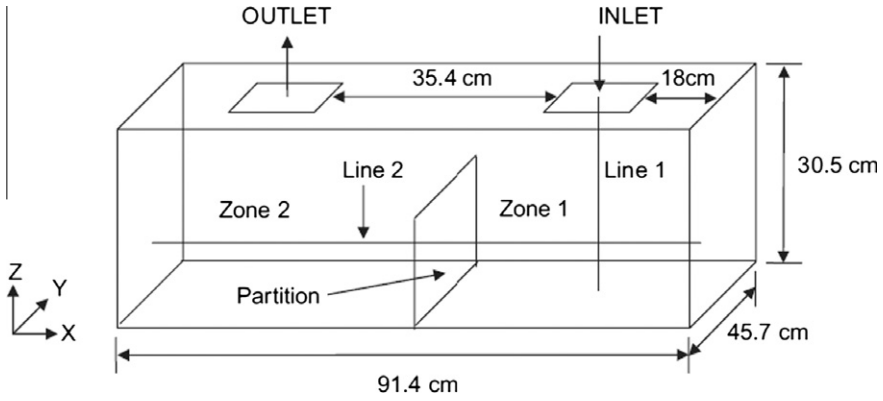

Fig. 9. Schematic of the scaled down room with its dimensions used in the experiments by Posner. This room has a partition which is representative of building office layouts that use partitions.

and V2F-Dav model agree well with the experimental data. Deviations are seen for the KW-based models. In contrast to the results for the two-dimensional free jet, all turbulence models over-estimate the turbulence kinetic energy and hence overestimate the shear and normal stresses. This is caused by the linear pressure-shear correlation term which produces too much turbulence kinetic energy in this region. The largest differences between experimental data and CFD simulations are generally found in the region between $y/y_{0.5} = 1$ and $y/y_{0.5} = 2$, which is the region furthest away from the jet center. Given that the turbulence stress redistribution in this region is not captured by the models, then it is expected that the spreading rate and any additional scalar transport will be affected (see Fig. 5).

The presence of the boundary wall and its associated damping of turbulence cause the spreading rate to be significantly lower than that of a free jet (see above). The calculated jet spreading rate $dy_{1/2}/dx$ is given in Table 4. All turbulence models overpredict the jet spreading rate comparison to the experimental data. This correlates with the direct link between the jet spreading rate and the turbulent shear stress. Best agreement was achieved by the RKE and the non-linear turbulence models.

3.3. Two-dimensional airflow

The IEA Annex 20 2D room geometry [24] is a test case, which has a jet diffuser at the ceiling. Fig. 6 shows the room layout and the planes where the flow profiles are taken, as well as the separation and reattachment points. The room dimensions are $H = 3$ m, $B = 3$ m, $L = 9$ m, $h = 0.168$ m and $t = 0.48$ m, where H is the height, B is the room width and L is the length of space. LDA measurements for this room were made by Nielsen et al. [25]. The Reynolds number based on the inlet height of the inlet is $Re = 5000$.

In the calculations the inlet and outlet channel were added as shown in Fig. 6 for stability reasons and to ensure well-defined boundary conditions (i.e. prevention of backflow in the inlet and outlet zone). The measured data provides two measured velocity profiles in the planes at $x = 1H$ and $x = 2H$. The flow was characterised as two-dimensional by Nielsen [24] but later results of Pedersen and Meyer [26] and Voigt [35] showed that in the region below the inlet three-dimensional effects arise. Thus verification of turbulence models not only considers the velocity profiles but also the location of separation and reattachment points. These phenomena are primarily driven by the distribution of turbulent stresses in the three-dimensional space, so that the following results can serve to review the two-and three-dimensional properties of the turbulence models investigated.

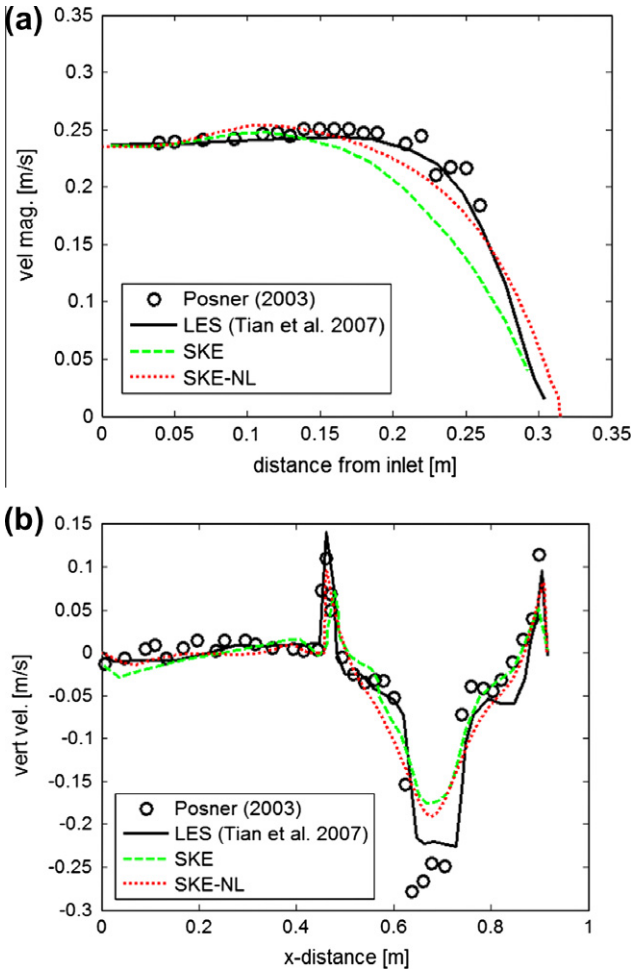

Fig. 10. Comparison between simulated and measured velocity components: (a) along the vertical inlet jet axis (line 1) and (b) along the horizontal line at mid-partition height (line 2).

The velocity profile results taken at $x = 1H$ and $x = 2H$ shown in Fig. 7 generally provide good agreement with the measurements for all models except for the KW-SST model. The high axial velocities close to the ceiling and the reverse flow in the bottom half of the room is captured well by the k–ε models and overestimated by the V2F-Dav model. The KW-SST model however, gives completely incorrect velocity profiles at $x = 1H$, but then recovers and matches

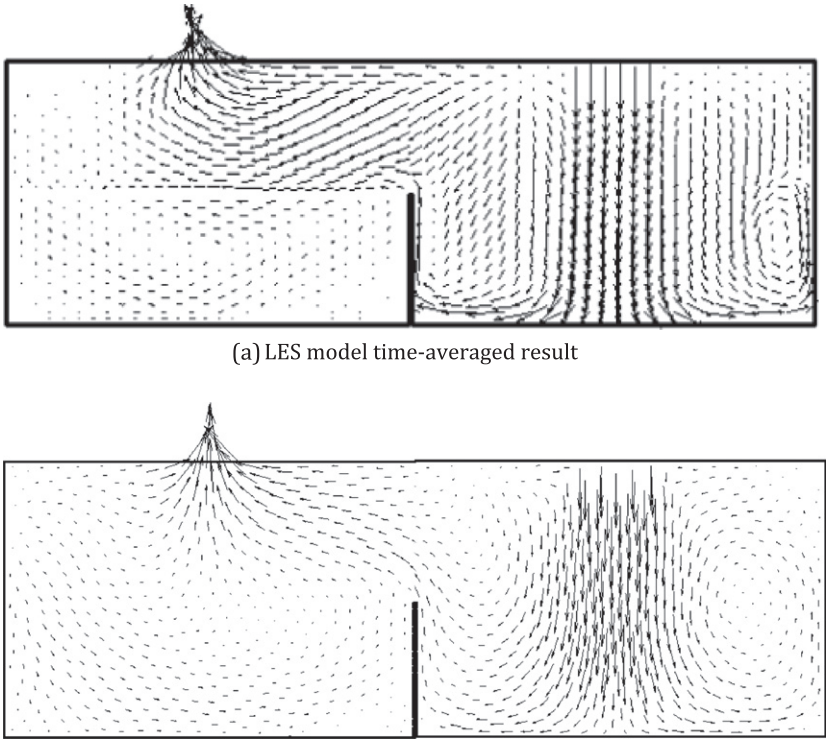

(a) LES model time-averaged result

(b) SKE-NL result.

Fig. 11. Predicted time-averaged air velocity vector field of the mid-plane (y = 0.2285 m) for the (a) LES model and (b) SKE-NL model simulation.

the experimental data better downstream at $x = 2H$. This suggests that the model has difficulties in resolving the secondary flows particularly in the region directly below the inlet.

Further investigations are performed and a vector and streamline plot is taken (Fig. 8) for a square region near the inlet with height and length of 1H. The experimental data from Pedersen and Meyer [26] show the presence of a recirculation zone in the lower left corner of the room. The size of the recirculation zone is well defined by the singular points on the left and bottom walls at $y/H = 0.55$ and $x/H = 0.9$. The calculated recirculation region show that the linear eddy viscosity models produce a small secondary vortex below the inlet area. The SKE model produces a smaller recirculation zone (bounded by $y/H = 0.26$, $x/H = 0.39$), with a qualitatively similar vector field but with a more dissipative nature, due to its linear eddy viscosity assumption. The vector field and streamline results for the RKE, RNG, and V2F-DAV models are very similar to that of the SKE model result and therefore are not presented. The KW-SST model produces a completely incorrect flow field. The recirculation zone in the lower left corner is present, however, it does not match with the experimental results at all. The results are substantially improved by the use of the nonlinear approach. The SKE-NL model captures the recirculation zone (bounded by $y/H = 0.7$, $x/H = 0.85$) well because of its ability to account for the anisotropic turbulence behaviour. It can be concluded that the turbulent normal stresses not only influence three dimensional flow (e.g. the turbulence induced secondary motion) but also has an influence on the flow pattern of the main airflow.

3.4. 3D room with partition

The room geometry has a floor area of 91.4 cm × 45.7 cm with a height of 30.5 cm. A partition with a height of 15 cm is located in the middle of the room. The inlet has the same size as the outlet, 10 cm × 10 cm. According to the experimental study of Posner [28], the inlet velocity (U_{inlet}) is 0.235 m/s with a uniform profile. Based on the inlet velocity and the inlet width, the Reynolds number of the inlet airflow is determined to be 1600. An LES simulation has been performed by the authors [34] and its results are reproduced here for comparison with the linear and nonlinear standard k–ε models.

Comparison of the predicted velocity magnitude along the vertical inlet jet axis (line 1 in Fig. 9) against the experimental data is presented in Fig. 10a. Good agreement is achieved for the LES model, although there is a marginal discrepancy at the end of the jet that could be caused by the numerical diffusion. The SKE velocity magnitude profile is predicted well near the jet inlet, but is somewhat underpredicted in the region far from the wall. The SKE-NL provides improved results with closer matching to the LES and experimental data. Fig. 10b shows the comparison between the predicted and measured vertical velocity component along the horizontal line at the mid-partition height (line 2 in Fig. 9). From the left wall to the partition, the results yield a smooth velocity profile where all CFD models agree well with the experiment data. In the region between the partition and the right wall the two peaks in the profiles (one near the left wall and one near the right wall) are captured reasonably well. The peak velocity near the left wall is caused by the partition while the peak near the right wall is caused by the nearby wall forcing a recirculation of the flow. A considerable dip in the profile is found underneath the jet location. Here the SKE and SKE-NL model are not able to capture the effect of the jet velocity penetration. Overall it must be noted that the SKE-NL improves the predicted results over the SKE model.

The simulated time-averaged velocity field at the mid-plane (y = 0.2285 m) of the model room is shown in Fig. 11. The main features of the flow including the jet stream from the inlet, the recirculation structures in the region next to the right wall (zone 1) and the region beneath the outlet are adequately predicted by the LES model. The vector plot for the SKE-NL model shows a similar general trend to the LES simulation. However in the region near the outlet it does not capture the flow distributing downwards which

is found in the LES simulation. The vector plot for the SKE model showed a near replica of the SKE-NL results and therefore is not shown here for brevity. The non-linear model developed was based on a calibration of the turbulence model coefficients with experiments and DNS data for jet flows. As such a limitation of this method is that it does not consider the exact flow physics in such conditions, and thus may be limited to conditions where jet flows are dominant.

4. Conclusion

In order to acquire new knowledge on the applicability of different turbulence models for mixed ventilation systems, a number of linear and non-linear turbulence models are applied to various model flows. Comparison of the measured and computed results of a plane free and wall jet, the flow through the IEA-Annex 20 room, and a 3D room with a partition showed that the proposed nonlinear eddy viscosity approach can improve the prediction of the turbulent normal stress distribution. The isotropic assumption of RANS models is reflected in the turbulent stresses whereby the anisotropic behaviour is not captured. This leads to failures in the secondary turbulence driven flow features. Improvements compared to the linear turbulence models were found with the v^2–f model and the modified k–ω model by Peng et al. [27]. Nevertheless, the v^2–f model fails in predicting the shear stress profile $u_1'u_2'$ for jet flows and hence delivers a lower spreading rate in comparison with experimental data. This is primarily caused by the correlation to determine the model constant C_{1s} and thus in future work the influence of this correlation has to be investigated. Non-linear versions of the standard k–ε and k–ω models were also presented which were able to reproduce the turbulence induced secondary flow. In the course of this work it could be shown that the proposed nonlinear approach avoids the well-known normal stress limits of the linear models while still preserving the inherent robustness of the linear eddy viscosity models (e.g. the simple calibration for shear flows, high numerical efficiency and stability etc.) so that these models are recommended for the simulation of linear diffuser flows.

References

[1] Abanto J, Barrero D, Reggio M, Ozell Bt. Airflow modelling in a computer room. Build Environ 2004;39:1393–402.
[2] Abrahamsson H. On turbulent wall jets, in Department of Thermo and Fluid Dynamics. Göteburg: Chalmers University of Technology; 1997.
[3] Abrahamsson A, Johansson B, Löfdahl L. A turbulent plane two-dimensional wall-jet in a quiescent surrounding. Eur J Mech B/Fluids 1994;13:533–6.
[4] Bäumer V. Ein Vergleich expliziter algebraischer Reynolds-Spannungsmodelle. Dissertation. Techn Universität Braunschweig; 2000. ISBN 3-8265-6979-2.
[5] Chen Q. Comparison of different k–ε models for indoor air flow computations. Numer Heat Trans, Part B: Fund 1995;28:353–69.
[6] Chen Q, Zhai Z. The use of CFD tools for indoor environmental design. In: Malkawi A, Augenbroe G, editors. Advanced building simulation. New York: Spon Press; 2004. p. 119–40.
[7] Cheong KWD, Djunaedy E, Poh TK, Tham KW, Sekhar SC, Wong NH, et al. Measurements and computations of contaminant's distribution in an office environment. Build Environ 2003;38:135–45.
[8] Chung KC. Three-dimensional analysis of airflow and contaminant particle transport in a partitioned enclosure. Build Environ 1999;34:7–17.
[9] Davidson L, Nielsen PV, Sveningsson A. Modification of the V2F model for computing the flow in a 3d wall jet. Turbul Heat Mass Trans 2003;4:577–84.
[10] De Souza FA, Nguyen D, Tavoularis S. The structure of highly sheared turbulence. J Fluid Mech 1995:303.
[11] Durbin PA, Pettersson Reif BA. Statsitical theory and modeling for turbulent flows. John Wiley & Sons, Ltd: New York, Weinheim, Brisbane, Singapore, Toronto; 2001. ISBN 0 471 49736 3.
[12] Fletcher CAJ. Computational techniques for fluid dynamics I fundamental and general techniques. Berlin, Heidelberg, NewYork: Springer; 2000. ISBN 3-54053058-4.
[13] Gatski TB. On explicit algebraic stress models for complex turbulent flows [microform]/Gatski TB, Speziale CG. National Aeronautics and Space Administration, Langley Research Center; National Technical Information Service, distributor, Hampton, Va: Springfield, Va, 1992.
[14] Gebremedhin KG, Wu BX. Characterization of flow field in a ventilated space and simulation of heat exchange between cows and their environment. J Therm Biol 2003;28:301–19.
[15] Gutmark E, Wygnanski I. The planar turbulent jet. J Fluid Mech 1976;73:465–95.
[16] Hwang RR, Jaw S-Y. Second-order closure turbulence models: their achievements and limitations. In: Proceedings of the National Science Council, Republic of China, Part A: Physical Science and Engineering, 1998.
[17] Isabey D, Chang HK. Steady and unsteady pressure-flow relationships in central airways. J Appl Physiol 1981;51:1338–48.
[18] Kim J, Moin P, Moser R. Turbulence statistics in fully developed channel flow at low Reynolds number. J Fluid Mech 1987;177:133–66.
[19] Laufer J. Investigation of turbulent flow in a two dimensional channel, Tech. Rep. 1053, NACA, 1951.
[20] Launder BE, Spalding DB. Lectures in mathematical models of turbulence. London, England: Academic Press; 1972.
[21] Lien F, Kalitzin G. Computations of transonic flow with the v2f turbulence model. Int J Heat Fluid Flow 2001;22:53–61.
[22] Lübcke HM, Rung T, Thiele F. Prediction of the spreading mechanism of 3D turbulent wall jets with explicit Reynolds-stress closure. Int J Heat Fluid Flow 2003:24.
[23] Menter FR. Two-equation eddy-viscosity turbulence models for engineering applications. Am Inst Aeronaut Astronaut J 1994;32:1598–605.
[24] Nielsen PV. Specification of a two-dimensional test case, Aalborg University, IEA Annex 20: air flow patterns within buildings, 1990.
[25] Nielsen PV, Restivo A, Whitelaw JH. The velocity characteristics of ventilated rooms. J Fluid Eng 1978;100:291–8.
[26] Pedersen JM, Meyer KE. Analysis of flow structures in an annex 20 room. 4th international symposium on particle image velocimetry. Göttingen, Germany; 2001.
[27] Peng SH, Davidson L, Holmberg S. Performance of two equation turbulence models for numerical simulation of ventilated rooms. In: Proceedings room ventilation 1996;2:153–60.
[28] Posner JD, Buchanan CR, Dunn-Rankin D. Measurement and prediction of indoor air flow in a model room. Energy Build 2003;35:515–26.
[29] Rouaud O, Havet M. Computation of the airflow in a pilot scale clean room using k–ε turbulence models. Int J Refrig 2002;25:351–61.
[30] Rubel A. On the vortex streching modification of the ke turbulence model: radial jets. AIAA J 1985;23:1129–30.
[31] Shih TH, Liou WW, Shabbir A, Yang Z, Zhu J. A new k–ε eddy viscosity model for high Reynolds number turbulent flows. Comput Fluids 1995;24:227–38.
[32] Tavoularis S, Corrsin S. Experiments in nearly homogenous turbulent shear flow with a uniform mean temperature gradient. Part 1. J Fluid Mech 1981;104:311–47.
[33] Tavoularis S, Karnik U. Further experiments on the evolution of turbulent stresses and scales in uniformly sheared turbulence. J Fluid Mech 1989;204:457–78.
[34] Tian ZF, Tu JY, Yeoh GH, Yuen RKK. Numerical studies of indoor airflow and particle dispersion by large eddy simulation. Build Environ 2007;42:3483–92.
[35] Voigt LK. Evaluating turbulence models for 3-D flows in encolure by topology. Montreal Canada: Ninth International IBPSA Conference; 2005.
[36] Wilcox DC. Turbulence modeling for CFD. 3rd ed. San Diego USA: DCW Industries, Inc.; 2006.
[37] Wolfshtein M. The velocity and temperature distribution in one-dimensional flow with turbulence augmentation and pressure gradient. Int J Heat Mass Transf 1969;12:301–18.
[38] Zhai Z. Application of computational fluid dynamics in building design: aspects and trends. Indoor Built Environ 2006;15:305–13.
[39] Zhang Z, Zhang W, Zhai Z, Chen Q. Evaluation of various turbulence models in predicting airflow and turbulence in enclosed environments by CFD: part-2: comparison with experimental data from literature. HVAC R Res 2007;13:871–86.